Microtubule depolymerization at kinetochores restricts anaphase spindle elongation

Geng-Yuan Chen[1], Changfeng Deng[2], David M. Chenoweth[2], Michael A. Lampson[1]*

[1]Department of Biology, University of Pennsylvania, Philadelphia, PA, 19104
[2]Department of Chemistry, University of Pennsylvania, Philadelphia, PA, 19104

*Corresponding author. Email: lampson@sas.upenn.edu

Abstract

Anaphase chromosome segregation depends on forces exerted by spindle microtubules. Current models propose two mechanisms of force generation: kinetochore microtubules (kMTs) depolymerize to pull chromosomes toward the spindle poles (anaphase A), while antiparallel microtubule sliding in the central spindle further separates the chromosomes by elongating the spindle (anaphase B). Experimental evidence in cells supports the sliding mechanism, but contributions of the depolymerization mechanism remain unclear. Here we show that kMT depolymerization limits spindle elongation rather than moving chromosomes apart. We developed a chemical optogenetic approach to recruit a microtubule depolymerase to kinetochores at anaphase onset, thereby increasing the rate of kMT depolymerization without perturbing earlier stages of mitosis. We find that increased depolymerization slows the velocity at which spindle poles move apart without changing kinetochore separation velocities. Our findings support a model in which kinetochores selectively couple to central spindle microtubules parallel to their kMTs, so that antiparallel sliding drives chromosome segregation while kMT depolymerization pulls poles inward.

Introduction

During cell division, sister chromosomes segregate in anaphase to partition the two replicated genomes into daughter cells. Three mechanisms of force generation in anaphase have been described. First, kinetochore-microtubule (kMT) bundles depolymerize to pull chromosomes and spindle poles toward each other. Second, antiparallel microtubule sliding in the central spindle pushes the two half-spindles apart. Third, astral microtubules pull spindle poles apart. Connections between these different microtubule populations make it difficult to dissect the contributions of potential force-generating mechanisms to chromosome segregation.[1]

Current "chromosome-pulled" models propose that depolymerizing kMTs pull each chromosome toward its attached pole (anaphase A) (**Fig. 1a**).[2-4] As chromosomes are pulled outward, antiparallel microtubule sliding pushes poles apart or pushes kMTs apart to elongate the spindle (anaphase B).[5,6] Astral microtubules can also pull poles apart, but antiparallel sliding is thought to be the primary mechanism driving anaphase B in human cells.[6] Molecular motors slide antiparallel microtubules apart *in vitro*, mimicking spindle elongation,[7-9] and laser ablation of the central spindle between sister

kinetochores in early anaphase slows kinetochore separation.[10,11] Furthermore, manipulations that increase or decrease antiparallel sliding velocities affect both anaphase spindle elongation and chromosome segregation velocities.[12-18] These findings demonstrate the importance of antiparallel sliding for chromosome segregation. In contrast, although depolymerizing microtubules can move tip-coupled objects (chromosomes or beads) in vitro,[3,4] the contribution of kMT depolymerization to anaphase chromosome segregation remains unclear. Manipulations that slow kMT depolymerization in cells, by inhibiting microtubule depolymerase activity, have the expected effect of decreasing the velocity of kinetochores and poles moving toward each other (anaphase A). However, chromosome segregation velocities have not been reported in these conditions.[19-24] In addition, depolymerases localize to microtubules beyond kMTs, so inhibition can affect multiple populations of spindle microtubules.[4]

In an alternative model, the central spindle is coupled to chromosomes so that antiparallel sliding directly drives anaphase chromosome segregation.[25] Neither kMT depolymerization (anaphase A) nor spindle elongation (anaphase B) is necessary for chromosome movements in this model. The spindle elongates because poles are attached to kMTs, so sliding moves poles outward, but chromosome movements are independent of spindle poles. We refer to this model as the "pole-pulled" model because kMT depolymerization at either kinetochores (plus-ends) or poles (minus-ends) pulls poles inward toward the chromosomes (**Fig. 1a**).[25] Spindle elongation is thus a combination of outward forces on spindle poles from antiparallel sliding and astral microtubules and inward forces from kMT depolymerization and potentially central spindle depolymerization. For example, if kMT depolymerization is fast enough, chromosomes can segregate without spindle elongation as in *C. elegans* meiosis.[26]

To distinguish between the chromosome-pulled and pole-pulled models, we designed a chemical optogenetic assay to acutely increase microtubule depolymerization at kinetochores in anaphase in human cells. We show that increased kMT depolymerization restricts pole separation without affecting chromosome separation, consistent with the pole-pulled model. We propose a molecular model in which each kinetochore selectively binds to the sides of central spindle microtubules in parallel orientation to its kMTs. Antiparallel sliding moves central spindle microtubules of opposite orientations apart, along with their bound kinetochores. As kMTs depolymerize, poles are pulled inward toward kinetochores anchored to the central spindle. To test this model, we developed additional chemical optogenetic assays to manipulate spindle checkpoint signaling and antiparallel sliding in the central spindle. We inhibited the checkpoint to induce anaphase on monopolar spindles.[27] Some sister kinetochore pairs localize near antiparallel microtubule bundles and move away from other in anaphase, consistent with antiparallel sliding driving their movements. We also recruited a microtubule-binding protein to the central spindle in anaphase to suppress antiparallel sliding. We find reduced kMT depolymerization, consistent with kinetochore linkage to the central spindle to constrain plus-end depolymerization. Overall, these results support our model in which kinetochores are mechanically coupled to central spindle microtubules oriented parallel to their kMTs, so that antiparallel sliding moves sister chromosomes apart while kMT depolymerization pulls poles inward.

Results

kMT depolymerization regulates spindle elongation

The chromosome-pulled model predicts that increasing kMT depolymerization in anaphase should increase kinetochore separation velocity, with no effect on pole separation velocity. Conversely, the pole-pulled model predicts decreased pole separation velocity as poles are pulled inward, with no effect on kinetochore separation velocity. To distinguish between these models, we designed an assay to increase the rate of microtubule depolymerization at kinetochores at anaphase onset. We recruited the motor domain of the microtubule depolymerase MCAK (Mitotic Centromere-Associated Kinesin; kinesin-13) to kinetochores using a photocaged small molecule that heterodimerizes HaloTag and *Escherichia coli* dihydrofolate reductase (eDHFR) fusion proteins.[28-30] We fused HaloTag to the kinetochore protein SPC25 (the anchor) and fused eDHFR to the MCAK motor domain (the effector), so that uncaging leads to dimerization and MCAK recruitment to kinetochores (**Fig. 1b-d**). This chemical optogenetic approach provides temporal precision by light activation and molecular specificity by using genetically tagged constructs.[31] By activating immediately after anaphase onset, our manipulations do not affect earlier stages of spindle formation and kinetochore attachment. As MCAK is active only at microtubule ends,[32] we expect that recruitment of the motor domain to kinetochores increases depolymerization of kMTs but not other proximal microtubules in the central spindle.

We first tested the kMT depolymerization assay in metaphase spindles, in which cohesion prevents sister kinetochores from moving farther apart. We find that MCAK recruitment leads to rapid spindle shortening, as poles move inward toward the kinetochores within 2 min of uncaging (**Fig. 1e-f, Supplementary Video 1**). This result indicates that MCAK recruitment increases kMT depolymerization as expected, and that kinetochores remain coupled to their attached kMTs.

To determine the effects of increased kMT depolymerization in anaphase, we recruited MCAK to kinetochores within 1 min after sister kinetochores start to move apart, indicating anaphase onset (**Fig. 2a-b, Supplementary Video 2**). We measured three distances at each time point: between separating kinetochores, between poles, and between kinetochores and their attached pole (**Fig. 2c**). For each cell, we fit a slope to the earliest time window exhibiting a linear range for all distances to measure velocities of pole separation (V_{PP}), kinetochore separation (V_{KK}), and kMT depolymerization (V_{PK}) (**Fig. 2d**). MCAK overexpression alone does not affect any of these velocities (**Supplementary Fig. 1**), and MCAK recruitment to kinetochores increases the rate of kMT depolymerization, as expected (V_{PK}, from 0.52 ± 0.03 μm/min to 0.77 ± 0.04 μm/min, mean ± SEM, **Fig. 2e**). Pole separation velocity decreases (V_{PP}, from 1.07 ± 0.08 μm/min to 0.40 ± 0.10 μm/min, mean ± SEM) with increased kMT depolymerization, but kinetochore separation velocity is not affected (**Fig. 2f-g**). The decrease in V_{PP} is double the increase in V_{PK}, which represents only half of the spindle, indicating that poles are pulled inward toward the kinetochores by depolymerizing kMTs as in metaphase (**Fig. 1e-f**). We conclude that kMT depolymerization restricts spindle elongation rather than moving chromosomes, consistent with the pole-pulled model.

To explain both outward forces on chromosomes and inward forces on poles, we propose a "sort and grip" model: each kinetochore sorts central spindle microtubules and selectively grips (binds tightly to the sides of) those in parallel orientation to the kMTs (**Fig. 2h**). As a result, antiparallel sliding moves kinetochores and their attached kMTs outward, while kMT depolymerization pulls poles inward relative to the central spindle where kinetochores are anchored. Forces exerted by kMT plus-end depolymerization rely on the well-established ability of kinetochores to maintain attachments to depolymerizing kMT plus-ends.[3] Sorting can be mediated by molecular motors, crosslinkers, or branching microtubule arrays that sort microtubules for the same polarity,[33,34] so that kinetochores selectively bind parallel central spindle microtubules based on proximity.

Anti-poleward motions in monopolar anaphase

To test the sort-and-grip model, we designed two additional chemical optogenetic assays to manipulate spindle checkpoint signaling and antiparallel sliding in the central spindle. First, we initiated anaphase on monopolar spindles by inhibiting the spindle assembly checkpoint using conditional pharmacology. The sort-and-grip model predicts that kinetochore motions depend on the arrangement of kMTs and adjacent antiparallel bundles. For some sister kinetochore pairs, kMTs orient in opposite directions on a monopolar spindle (**Fig. 3a**).[35] In this configuration, antiparallel sliding would move sister kinetochores away from each other rather than moving both sisters toward the pole. To induce anaphase, we used a photocaged inhibitor of the checkpoint kinase MPS1 (Monopolar Spindle 1) linked to the Halo ligand, which binds covalently to the Halo-tagged kinetochore anchor SPC25 (**Fig. 3b**).[36] MPS1 is inhibited only after uncaging with a pulse of light. As the inhibitors are bound to SPC25 and do not diffuse between cells, local uncaging triggers anaphase in one cell at a time. This approach allows sequential live imaging of individual cells with high temporal resolution.

After MPS1 inhibition, we examined localization of the antiparallel microtubule crosslinker PRC1 (Protein Regulator of Cytokinesis 1), which marks antiparallel bundles.[14,37,38] PRC1 signals gradually decrease in length and increase in intensity, indicating antiparallel sliding that decreases the overlap length in each bundle (**Supplementary Fig. 2**), as observed in the central spindle in normal bipolar anaphase[14,37,38] and in reconstituted systems.[39-41] We analyzed kinetochore motions separately for sister pairs either colocalized to (on-bundle) or away from (off-bundle) PRC1 signals (**Fig. 3c-f, Supplementary Videos 3-4**). Off-bundle pairs exhibit minimal movement of sisters away from each other, consistent with a lack of separation forces by antiparallel sliding. Conversely, some on-bundle sisters move apart, with the distal kinetochore of these pairs moving away from the pole (**Fig. 3g**). This result is consistent with the sort-and-grip model, in which antiparallel sliding drives chromosome movements depending on local spindle organization near kinetochores, independent of spindle poles. As monopolar spindles are generated by inhibiting kinesin-5 motors, antiparallel sliding is likely due to kinesin-4 (KIF4A) motors recruited to PRC1 bundles.[15] Previous findings, using laser ablation to detach one kinetochore from its attached pole

in a bipolar spindle, also show sister kinetochore separation consistent with the sort-and-grip model.[11]

Suppressed central spindle sliding inhibits kMT depolymerization

In the sort-and-grip model, kMT plus ends are coupled to the central spindle via side-attached kinetochores. Without antiparallel sliding to move kinetochores outward, kMT depolymerization would require shortening the spindle by pulling poles inward, against outward forces exerted on poles by astral MTs. Thus, we predict that suppressed antiparallel sliding would reduce kMT depolymerization because both kMT plus and minus ends are constrained.

To suppress antiparallel sliding, we generated "brake" complexes in the central spindle. We fused HaloTag to full-length dimeric PRC1 (the anchor) and fused eDHFR to a monomeric PRC1 truncation mutant (PRC1M, the effector) that binds to microtubules without crosslinking activity on its own. Uncaging generates brake complexes by recruiting PRC1M to dimeric PRC1 bound to antiparallel bundles, which should strengthen PRC1 binding to microtubules and thus increase friction to suppress sliding within the bundle (**Fig. 4a-b**). Before uncaging, PRC1M binds to microtubules proportional to local microtubule density, with a subtle enrichment around the equator (**Fig. 4c, Supplementary Video 5**). This enrichment increases after activation, consistent with recruitment to PRC1-labeled antiparallel bundles in the central spindle.[14,37,38]

PRC1 itself acts as a molecular brake, as it restricts microtubule sliding *in vitro,*[39-41] and its depletion in cells increases the separation velocity of the two half-spindles.[14,42] Thus, we predict increased friction and suppressed antiparallel sliding due to PRC1 overexpression alone, followed by a further increase in friction after uncaging and PRC1M recruitment at anaphase onset. We measured kinetochore and pole velocities and kMT depolymerization as in Fig. 2c-d. We find that PRC1 overexpression decreases pole and kinetochore separation velocities, proportional to PRC1 levels on spindles, and PRC1M recruitment further decreases these velocities (**Fig. 4d-e**, **Supplementary Fig. 3a-c, Supplementary Video 6**). These results indicate progressively greater suppression of antiparallel sliding as expected. The rate of kMT depolymerization decreases as antiparallel sliding is suppressed, with the slowest rate observed in the presence of both PRC1 overexpression and PRC1M recruitment (**Fig. 4f, Supplementary Fig. 3d**). This result is consistent with the sort-and-grip model. The plus-ends of kMTs are coupled to the central spindle, while the minus-ends are anchored at the poles and constrained by astral MTs, so kMTs are not free to depolymerize.

Discussion

Using chemical tools to manipulate spindle organization and specific microtubule populations within the spindle, our experiments support a model in which antiparallel sliding directly drives anaphase chromosome segregation while kMT depolymerization limits spindle elongation. We first show that enhanced kMT depolymerization slows pole separation without increasing kinetochore separation (**Fig. 2**). Based on these findings,

220 we propose a sort-and-grip model (**Fig. 5**): parallel microtubule sorters position
221 kinetochores close to central spindle microtubules oriented parallel to the kMTs, so that
222 kinetochores selectively grip these central spindle microtubules upon anaphase onset. If
223 sorting is established before anaphase onset, then sorters can be absent in anaphase
224 or allow sliding of kMTs relative to the central spindle. Kinetochores grip tightly in
225 anaphase, however, without sliding on the central spindle, which has two key outcomes.
226 First, antiparallel sliding in the central spindle moves sister kinetochores apart together
227 with their attached kMTs. Second, kMT plus-end depolymerization pulls kMTs and poles
228 inward toward kinetochores that are tightly coupled to the central spindle, against
229 outward movement of kMTs driven by anti-parallel sliding. Depolymerization of kMT
230 minus-ends also pulls poles inward in this model. Our results from two additional assays
231 support the sort-and-grip model. First, sister kinetochores can move apart on monopolar
232 spindles, consistent with antiparallel sliding moving sorted microtubules together with
233 their gripped kinetochores (**Fig. 3**). Second, suppressed antiparallel sliding slows kMT
234 depolymerization, indicating that kinetochores couple to the central spindle (**Fig. 4**).
235 Velocity measurements in multiple model systems are consistent with the sort-and-
236 grip model. In human cells, *C. elegans* oocytes and embryos, and *Xenopus* egg
237 extracts, antiparallel sliding velocity within the central spindle matches kinetochore
238 velocity in anaphase (**Supplementary Fig. 4a**)[10,43], suggesting that antiparallel sliding
239 moves chromosomes without requiring a contribution from kMT depolymerization.
240 Sliding velocity also correlates with poleward movements of kMTs.[11,15] In addition,
241 slowing kMT depolymerization, by depleting microtubule depolymerases or severing
242 enzymes in human cells or adding non-degradable cyclin B to *Xenopus* egg extracts,
243 increases spindle elongation velocity.[20,24,44] These results are consistent with kMT
244 depolymerization pulling poles inward and with our findings that increasing kMT plus-
245 end depolymerization slows spindle elongation (**Fig. 2**).
246 Microtubule severing experiments in multiple systems are also consistent with the
247 sort-and-grip model. Cutting the central spindle early in anaphase transiently halts
248 kinetochore separation in human cells and *C. elegans* oocytes and embyros,[10] whereas
249 kinetochores continue to separate after ablating centrosomes or microtubules midway
250 between kinetochores and their attached poles in human, *C. elegans*, rat-kangaroo,
251 newt, grasshopper, and crane-fly cells.[10,11,45-50] These findings indicate that antiparallel
252 sliding directly moves chromosomes. Structurally, central spindle microtubules are close
253 to kinetochores and their attached kMTs in high-resolution optical and EM images,[10,51,52]
254 and kMT perturbations by microneedle manipulation or microtubule severing suggest
255 crosslinking to the central spindle near chromosomes.[11,53-55] Kinetochores can thus
256 directly bind to the central spindle or interact with microtubule-associated proteins on
257 the central spindle to make the coupling robust.
258 To move chromosomes toward their attached poles correctly, the sort-and-grip
259 model relies on kinetochores attaching selectively to the sides of central spindle
260 microtubules oriented parallel to their kMTs (**Fig. 5**). This selectivity can be mediated by
261 microtubule sorting mechanisms acting earlier in mitosis that position kMTs adjacent to
262 parallel microtubules in the central spindle. In prometaphase, short microtubules bind
263 kinetochores at their plus-ends, while the minus-ends interact with antiparallel bundles

in the central spindle.[56] Minus-end directed motors sort these nascent kMTs and establish parallel coupling to central spindle microtubules to biorient sister kinetochores (**Supplementary Fig. 4b**).[57] Alternatively, minus-end directed motors also sort newly-grown microtubules in the central spindle poleward through kMTs (**Supplementary Fig. 4c**).[58] Furthermore, parallel microtubule arrays can assemble by growing microtubules from existing microtubule templates.[33,59-61] Microtubules nucleated from sister kMTs can thus grow toward the equator to generate a "bridging fiber" by antiparallel crosslinking (**Supplementary Fig. 4d**).[11] We propose that parallel microtubules sorted before anaphase persist so that kinetochores couple to these microtubules and move by antiparallel sliding in anaphase. Inhibition or depletion of potential candidates for these sorting mechanisms (e.g. augmin,[62] NuMA,[63] ZW10,[64] and kinesin-14[65]) commonly causes anaphase chromosome segregation errors, which can arise from incorrect kinetochore coupling to microtubules antiparallel to their kMTs.

Restricting spindle elongation may be important for later stages of division, when excessive spindle elongation is associated with midzone buckling and defocused cytokinetic furrows.[14,37,38,66-70] In addition, spindle poles act as hubs for numerous biochemical and mechanical cues,[71-73] so restricted spindle elongation may regulate pole communication with spindle midbodies or the cytokinetic furrow. Hence, telophase biology likely requires coordination between pole separation and chromosome separation velocities via depolymerizing kMTs.

Methods

Synthesis, characterization, and storage of chemical optogenetic probes. The photoactivatable dimerizer (CTH)[29,30] and photoactivatable localized MPS1 inhibitor (CRH)[36] were prepared as previously described. Both compounds were dissolved in DMSO at 20 mM and stored as 1 μL aliquots in amber plastic microcentrifuge tubes at -80 °C.

Small molecule inhibitors. All stocks were dissolved in DMSO and stored at -20 °C. Stock concentrations include 20 mM S-Trityl-L-Cysteine (STLC, Eg5 inhibitor; Sigma Aldrich) and 10 mM Verapamil (Tocris). Fresh aliquots were used for all experiments.

Plasmids. The pEM705 backbone with a CAG promoter was used to clone all plasmids for anchors and effectors.[74] The kinetochore anchor SPC25, fused to three tandem copies of HaloTag and an eGFP on its N-terminus (3×Halo-GFP-SPC25), was used as previously described.[29,30] To manipulate central spindle mechanics, PRC1 was used as an anchor, fused to 3× HaloTag with the far-red fluorescent reporter, miRFP670nano3 (hereafter denoted 670nano3), on its N-terminus (3×Halo-670nano3-PRC1).

All effectors were designed based on the construct with the red fluorescent protein mScarlet fused to the N terminus of *Escherichia coli* dihydrofolate reductase DHFR (mScarlet-eDHFR). For targeted microtubule depolymerization, the phospho-resistant motor domain of human MCAK ($MCAK_{179-583;S192A}$) was fused to the N terminus of mScarlet-eDHFR (MCAK-mScarlet-eDHFR).[30,75] To suppress microtubule sliding, a

307 monomeric PRC1 mutant (PRC1M, $PRC1_{341-620}$)[76] was fused to the C terminus of
308 mScarlet-eDHFR to make mScarlet-eDHFR-PRC1M.
309 To label spindle poles, a single copy or two tandem copies of the PACT (Pericentrin
310 and AKAP Centrosome Targeting)[77] domain was fused to eGFP (PACT-GFP or
311 2×PACT-GFP) in the pcDNA3.1 backbone containing cytomegalovirus and T7
312 promoters. To label the central spindle, full-length PRC1 was fused to two tandem
313 copies of 670nano3 (2×670nano3-PRC1), using pEM705 as the backbone.
314
315 **Cell cultures and transfection.** HeLa RMCE (recombination-mediated cassette
316 exchange) acceptor cells were passaged at 37°C in the growth medium containing
317 DMEM (Gibco) supplemented with 10% Fetal Bovine Serum (Clontech) and 1%
318 penicillin/streptomycin (Life Technologies), within 5% CO_2 atmosphere and humidity.
319 For assays, cells were cultured on coverslips (Bellco) coated by poly-D-lysine (Sigma-
320 Aldrich) for at least 16 h, and then transfected with the desired constructs using
321 Lipofectamine 3000 (Invitrogen) in Opti-MEM (Gibco) for at least 24 h.
322 Manipulations of mechanics and biochemistry at kinetochores were conducted with
323 cells stably expressing 3×Halo-GFP-SPC25, as previously described.[29,30] For the
324 monopolar anaphase assay, cells were transfected with 0.5-1 μg 2×670nano3-PRC1
325 and 250 ng PACT-GFP to mark the central spindle and spindle poles, respectively. For
326 kMT depolymerization, cells were transfected with 1-1.5 μg MCAK-mScarlet-eDHFR
327 and 250 ng 2×PACT-GFP.
328 Manipulations of central spindle mechanics were conducted with cells transiently
329 transfected with 0.6 μg Scarlet-eDHFR-PRC1M and 0.6 μg 3×Halo-670nano3-PRC1,
330 together with 100 ng CenpB-GFP and 250 ng PACT-GFP for labeling centromeres and
331 poles, respectively.
332
333 **Photoactivation and dimerization.** For recruitment experiments, cells were placed in a
334 magnetic chamber (Chamlide CM-S22-1; LCI) and incubated with growth medium and
335 CTH for 1 h. Unbound CTH was washed out by incubating for 20 min in imaging
336 medium containing L15 without phenol red (Gibco) (imaging medium) plus 10% FBS
337 and 1% penicillin/streptomycin. The medium was then replaced with fresh imaging
338 medium, and the chamber was moved to a stage in a 37°C environmental chamber
339 (PeCon). For dimerization experiments, cells were imaged live to determine the time of
340 anaphase onset. CTH was activated within 1 min after sister kinetochores started to
341 move apart, using a 405-nm laser (CrystaLaser LC) controlled by iLas2 software (Roper
342 Scientific) installed on MetaMorph (Molecular Devices), as previously described.[30]
343 Activation was performed over the entire cell at 25% laser power with 5 repetitions. To
344 induce anaphase in monopolar cells, cells were incubated with 10 μM Verapamil (an
345 efflux pump inhibitor) and 20 μM STLC in growth medium for 2 h, then 20 μM CRH was
346 added for 1 h. Unbound CRH was washed out by incubating in imaging medium with
347 STLC for 30 min. CRH was uncaged by a 5-second light pulse using a mercury arc
348 lamp filtered at 385/11 nm, and imaging started 15-20 min later. Procedures with light-
349 sensitive molecules were performed under red light in the room.
350

Image acquisition. Live cells at 37 °C were imaged with a confocal microscope (DM4000; Leica), equipped with a 100× 1.4 NA oil immersion objective (Leica), an XY Piezo-Z stage (Applied Scientific Instrumentation), a CSU10 spinning disk (Yokogawa), an electron multiplier charge-coupled device camera (ImageEM; Hamamatsu Photonics), and a 4-line laser module (405 nm, 488 nm, 561 nm, and 639 nm; Vortran Stradus VersaLase 4), as previously described.[30] Images were acquired with a 10-60s time interval, with 0.5-2 μm spacing for z-stacks covering 6-15 μm total. For dimerization experiments, cells were activated after image acquisition at t=0. For monopolar anaphase assay, images were acquired 15 minutes after uncaging.

Data analyses and statistical tests.

For monopolar anaphase cells, both kinetochores and poles were tracked by the Fiji::MTrackJ plug-in. In each frame, the distances of two sisters relative to the pole were calculated (D_{PK}). The distance difference between the two sisters (ΔD_{PK}) represents the inter-kinetochore distance along the axis between the pole and kinetochores (D_{KK}). For each trajectory, the maximum kinetochore separation velocity (max V_{KK}) represents the maximal displacement of inter-kinetochore distance (D_{KK}) across all possible one-minute time windows. A cutoff was defined as the 95% percentile of max V_{KK} of off-bundle sister kinetochore pairs.

For bipolar anaphase cells, the coordinates of kinetochores and spindle poles were measured by the Fiji::TrackMate and Manual Tracking plug-ins, respectively. Kinetochore coordinates were projected to the mitotic axis defined by poles, and then grouped based on their closest pole. In each frame, the median position of each group represents the centroid of projected kinetochores. Initial velocities were defined by the time window exhibiting linear displacement between the two poles (V_{PP}), between the two kinetochore centroids (V_{KK}), and between a kinetochore centroid and its corresponding pole ($-V_{PK}$). Cells were included in the analysis only if they exhibit constant kinetochore separation velocity at early time points, representing complete loss of cohesion and separation of sister chromosomes. To measure PRC1 intensity on a bipolar spindle, image stacks were mean-projected along z. Spindle-bound PRC1 signal was defined by the intensity within the minimal circle encompassing both spindle poles, with cytosolic intensity subtracted as background, summed for each cell. For each set of experiments, PRC1 intensities across different perturbations were normalized relative to the mean intensity of cells expressing 3×Halo-670nano3-PRC1.

Data from measurements were analyzed by MATLAB. Two-tailed Student's t-test was used to compare measurements between groups.

Acknowledgments: We thank the Philly ChromoClub and the Penn Center for Genome Integrity for discussions. This work was supported by the NIH (GM122475 and P01-CA265794) and the Basser Center for BRCA.

Author contributions: GYC designed and conducted cell biology experiments and wrote the manuscript. CD and DMC synthesized and characterized chemical optogenetic probes. MAL designed experiments and edited the manuscript.

Competing interests: The authors claim no competing financial interests.

Materials & Correspondence. Cell lines, chemicals, and protocols are available upon request. The corresponding authors adhere to the NIH Grants Policy and Sharing of Unique Research Resources. Correspondence and requests for materials should be addressed to MAL (lampson@sas.upenn.edu).

Supplementary Information is available for this paper.

Data availability. The datasets generated and analyzed during the current study are available from the corresponding author on reasonable request without restriction.

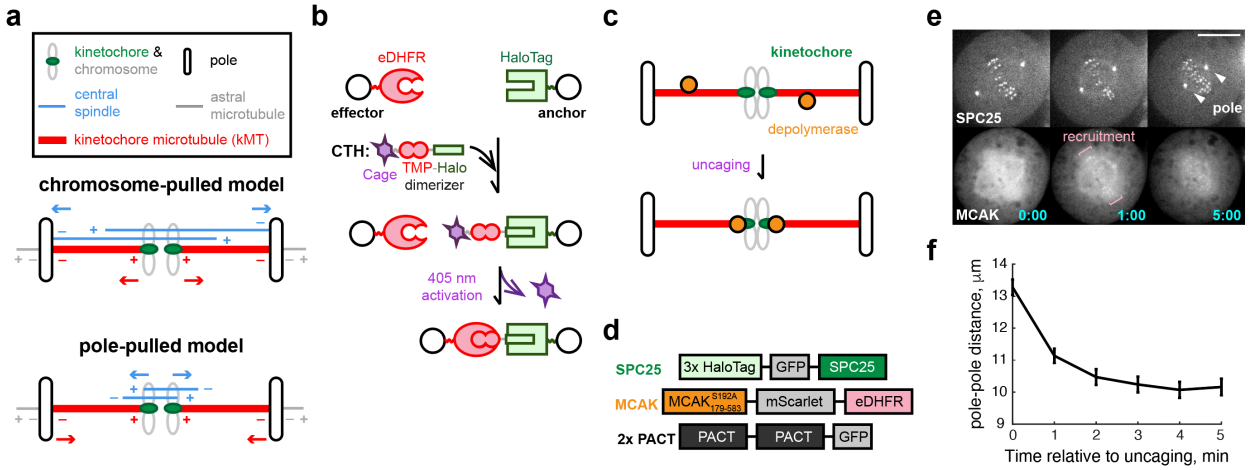

Figure 1. Induced kMT depolymerization shortens metaphase spindle. (a) Mechanical models for anaphase chromosome segregation. Polarity of antiparallel microtubules in the central spindle (blue), kMTs (red), and astral microtubules (gray) is indicated, with minus-ends (–) and plus-ends (+) facing toward and away from poles, respectively. In the chromosome-pulled model, antiparallel sliding in the central spindle pushes poles or kMTs apart (blue arrows), while kMT depolymerization pulls each chromosome outward toward its attached pole (red arrows). In the pole-pulled model, the central spindle couples to chromosomes, so antiparallel sliding directly moves sister chromosomes apart (blue arrows), and kMT depolymerization pulls poles inward toward the chromosomes (red arrows). **(b)** Schematic of light-inducible dimerization. The photocaged dimerizer (CTH) includes a Halo ligand (green) linked to the eDHFR ligand trimethoprim (TMP, red) and a photocage (purple). The dimerizer is activated by uncaging to make TMP accessible to eDHFR, recruiting the eDHFR-tagged effector to the Halo-tagged anchor. **(c)** Schematic of kMT shortening assay in metaphase. The microtubule depolymerase MCAK (orange) is recruited to kinetochores (green) after dimerizer uncaging at t=0 to enhance kMT depolymerization. **(d)** Constructs for kMT shortening assay. The minimal microtubule depolymerization domain ($MCAK_{179\text{-}583}$) was used, with a mutation to prevent phosphorylation: S192A. SPC25 is the kinetochore anchor, and PACT labels spindle poles. **(e-f)** Metaphase kMT shortening assay for cells expressing Halo-GFP-SPC25, PACT-GFP, and MCAK-mScarlet-eDHFR. Representative images (e) show kinetochores, poles, and MCAK recruitment after dimerization at t=0. Pole-pole distances (f) were measured for each cell and averaged at every time point (n=29 cells pooled from four independent experiments). Time stamps, min:s. Scale bars, 10 μm. Error bars: mean ± SEM.

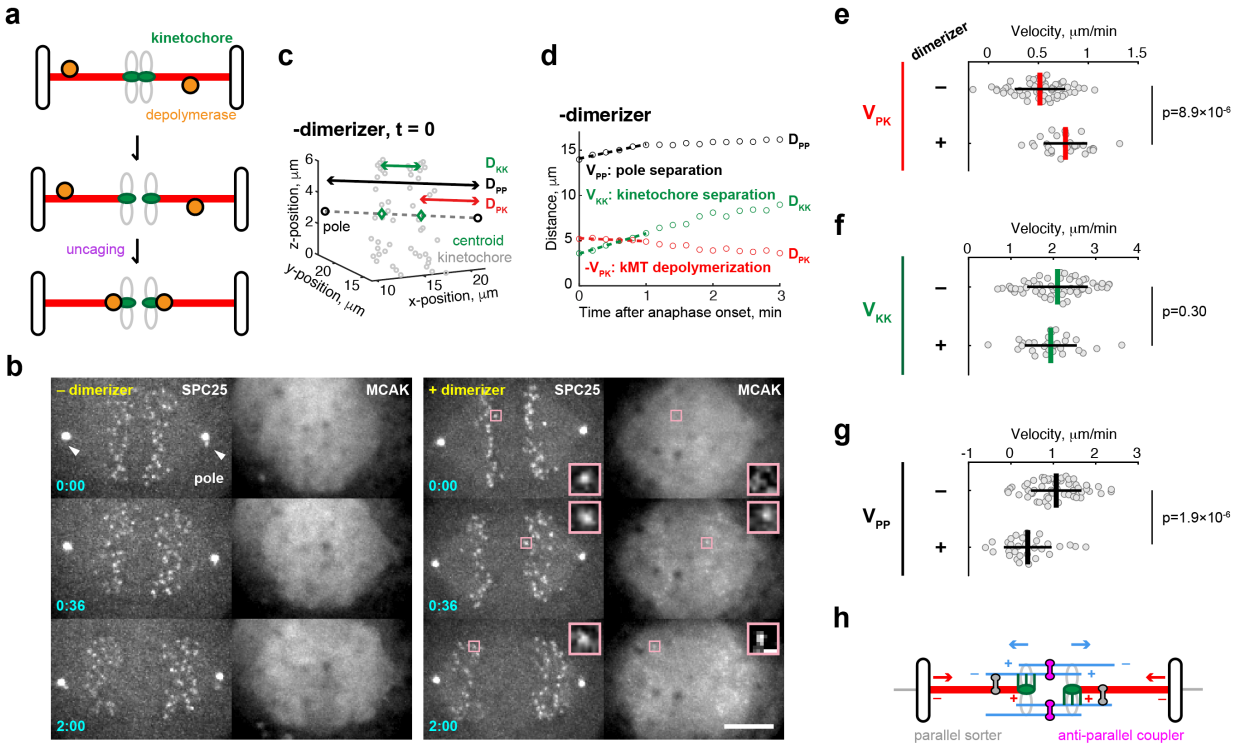

Figure 2. Enhanced kMT depolymerization slows pole separation in anaphase. (a) Schematic of kMT shortening assay in anaphase. The microtubule depolymerase MCAK (orange) is recruited to kinetochores (green) after dimerizer uncaging at t=0 at anaphase onset. **(b)** Representative images show cells expressing Halo-GFP-SPC25, MCAK-mScarlet-eDHFR, and PACT-GFP, with or without dimerization at t=0, immediately after sister kinetochores start to move apart. Contrast in the mScarlet channel was adjusted in each image to visualize MCAK recruitment. Insets for +dimerizer cells show kinetochores and MCAK recruitment at higher magnification with enhanced contrast. Time stamps, min:s. Scale bars, 5 μm or 500 nm in insets. **(c-d)** Analyses of kinetochore and pole motions. Example snapshot at t=0 (c) shows coordinates of poles (black) and kinetochores (gray circles). A pair of kinetochore centroids (green) represents the median positions of the two separating kinetochore masses projected to the mitotic axis (gray dashed lines, defined by the two poles). Three distances were calculated based on these coordinates: between kinetochore centroids (D_{KK}, green), between poles (D_{PP}, black), and between each kinetochore centroid and its adjacent pole (D_{PK}, red). Example traces (d) show distances over time, with initial velocities (dashed lines) measured in the earliest time window exhibiting linear increases of all three distances. **(e-g)** Initial velocities were calculated for kMT depolymerization (e), kinetochore separation (f), and pole separation (g) (n=58 cells – dimerizer pooled from six independent experiments, 30 cells +dimerizer pooled from seven independent experiments). Each data point represents a single cell. Lines: mean ± SD. **(h)** The sort-and-grip model proposes that parallel sorters (gray dumbbells) position kMTs (red) adjacent to parallel microtubules in the central spindle (blue). Kinetochores (green) grip adjacent microtubules, which are in the correct orientation for antiparallel sliding (mediated by antiparallel couplers/motors, magenta dumbbells) to

460 move sister kinetochores apart (blue arrows). Depolymerization at kMT plus-ends pulls
461 poles inward toward kinetochores (red arrows) that are coupled to the central spindle.
462

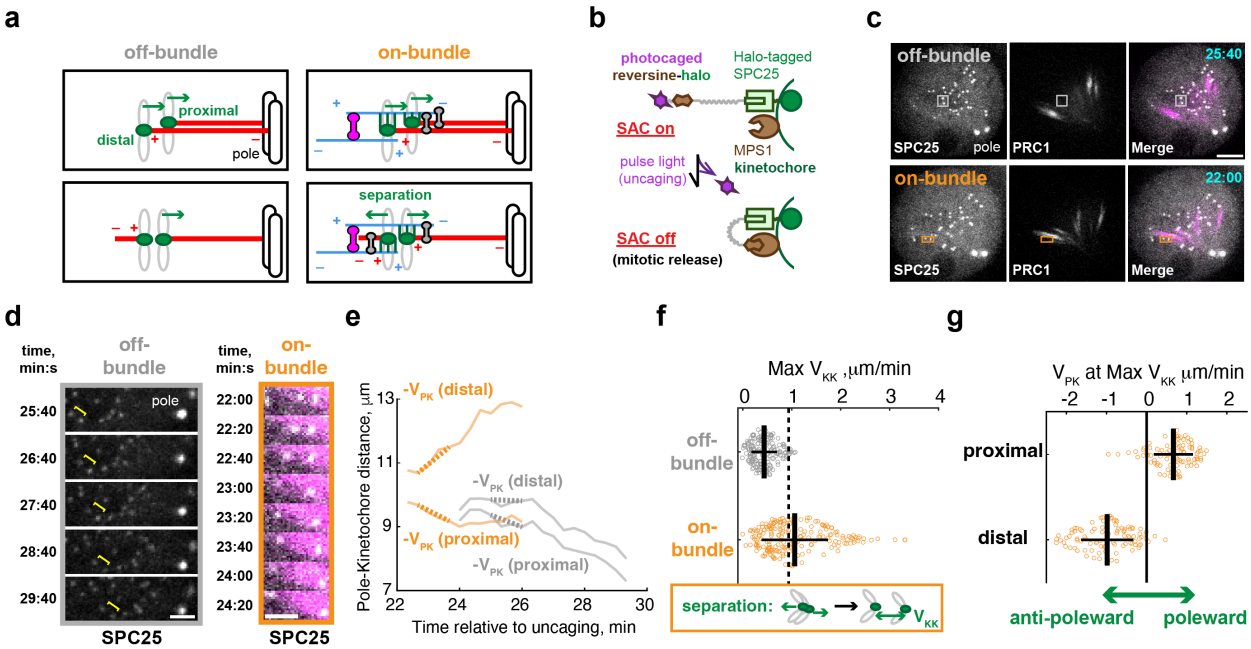

Figure 3. Anti-poleward kinetochore motions in monopolar anaphase. (a) Schematic of monopolar anaphase. Sister kinetochore pairs can localize away from or close to antiparallel bundles (off-bundle or on-bundle, respectively). Both kinetochores can attach to the pole (top panels), or the kMTs of the distal kinetochore can orient away from the pole (bottom panels). In the latter case, the sort-and-grip model predicts that antiparallel sliding can move the proximal and distal kinetochores toward and away from the pole, respectively, as kinetochores grip microtubules in parallel orientation to their kMTs (bottom right panel). Green arrows represent directions of kinetochore movement. **(b)** Schematic illustrates the conditional pharmacology approach for spindle checkpoint silencing in single cells. The MPS1 inhibitor (reversine, brown) is linked to a photocage (purple) and a Halo ligand (light green). The caged inhibitor localizes to kinetochores by binding to the Halo-tagged kinetochore protein SPC25 (green) and inhibits MPS1 (brown) only after uncaging. **(c-d)** Representative images (c) show HeLa cells expressing Halo-GFP-SPC25 (kinetochores), PACT-GFP (spindle poles), and 670nano3-PRC1 (antiparallel bundles), incubated with the kinesin-5 inhibitor STLC to create monopolar spindles. Time-lapse images (d) show representative off-bundle and on-bundle pairs, boxed in c. Yellow line: distance between the off-bundle sisters; time stamps (min:s): time after uncaging at t=0. **(e)** Individual kinetochore movements relative to the pole for the off-bundle (gray) and on-bundle (orange) sister pairs shown in d. Kinetochore velocity relative to the pole (V_{PK}) was calculated as the displacement within a one-minute time window, with poleward motion defined as the positive direction. Dashed lines represent the maximal velocity of sister kinetochore separation (Max V_{KK}). **(f)** Max V_{KK} plotted for off-bundle (n=168) and on-bundle (n=204) sister kinetochore pairs, from 23 cells pooled from seven independent experiments. Dashed line: upper bound for pairs that behave as off-bundle (95th percentile of the Max V_{KK} distribution for off-bundle pairs). Some on-bundle pairs separate with high V_{KK} as shown in e (orange traces). **(g)** For each on-bundle pair with Max V_{KK} above the dashed line (n=93 pairs),

491 indicating functional interactions with the bundle, V_{PK} is plotted for the proximal and
492 distal sisters. Black lines: mean ± SD. Scale bars, 5 μm in c or 2 μm in d.
493

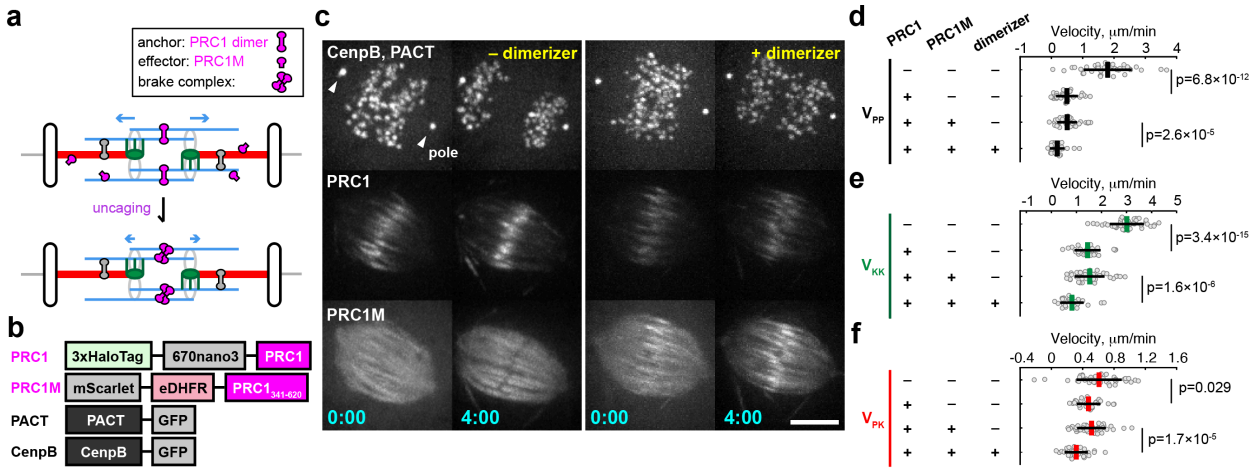

Figure 4. Suppressed bundle sliding inhibits kMT depolymerization. (a) Schematic of braking assay: monomeric PRC1 (PRC1M, magenta half-dumbbells) is recruited to dimeric PRC1 (magenta dumbbells) after uncaging at t=0, forming "brake" complexes to suppress antiparallel sliding (shown by reduced size of blue arrows). **(b)** Constructs for braking assay. PRC1M ($PRC1_{341\text{-}620}$) is truncated to remove the N-terminus. PACT and CenpB label spindle poles and kinetochores, respectively. **(c)** Representative images of cells expressing CenpB-GFP, PACT-GFP, Halo-670nano3-PRC1, and mScarlet-eDHFR-PRC1M with or without dimerization at t=0, immediately after anaphase onset. Time stamps min:s; scale bars, 5 μm. **(d-f)** Initial velocity analyses for pole separation (d), kinetochore separation (e), and kMT depolymerization (f). From top to bottom in each panel: n=39 control cells (without Halo-670nano3-PRC1 or mScarlet-eDHFR-PRC1M), n=28 with Halo-670nano3-PRC1, n=42 with Halo-670nano3-PRC1 and mScarlet-eDHFR-PRC1M but no dimerization, n=27 with Halo-670nano3-PRC1 and mScarlet-eDHFR-PRC1M and dimerization. All cells express CenpB-GFP and PACT-GFP. Cells were pooled from three independent experiments; each data point represents a single cell. Lines: mean ± SD.

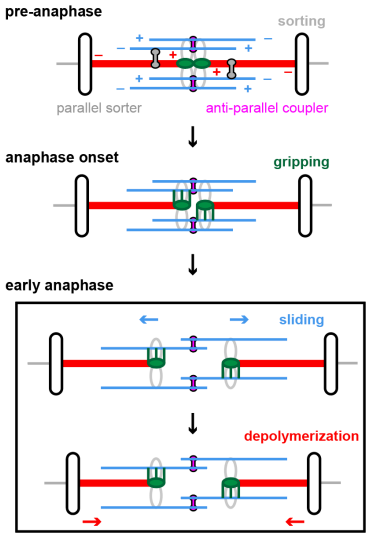

Figure 5. Proposed sort-and-grip processes. Before anaphase onset, microtubule sorting mechanisms position kMTs (red) close to parallel microtubules in the central spindle (blue) by parallel sorters (gray dumbbells). Upon anaphase onset, kinetochores (green) grip adjacent microtubules, which are correctly oriented for antiparallel sliding to move sister kinetochores apart. Parallel sorters are not needed after anaphase onset and are not shown for simplicity. Two concurrent processes drive pole and kinetochore movements in anaphase: antiparallel sliding directly separates gripped kinetochores, while microtubule depolymerization at kinetochores pulls poles inward toward kinetochores. The processes are shown sequentially for clarity but can occur simultaneously.

References

1. Maiato, H. & Lince-Faria, M. The perpetual movements of anaphase. *Cell Mol Life Sci* **67**, 2251-69 (2010).
2. Alberts, B. et al. in *Molecular Biology of the Cell*, Vol. seventh edition 1027-88 (W. W. Norton & Company, 2022).
3. Asbury, C.L. Anaphase A: Disassembling Microtubules Move Chromosomes toward Spindle Poles. *Biology (Basel)* **6**, 15 (2017).
4. McIntosh, J.R. Anaphase A. *Semin Cell Dev Biol* **117**, 118-126 (2021).
5. Scholey, J.M., Civelekoglu-Scholey, G. & Brust-Mascher, I. Anaphase B. *Biology (Basel)* **5**, 51 (2016).
6. Vukusic, K. & Tolic, I.M. Anaphase B: Long-standing models meet new concepts. *Semin Cell Dev Biol* **117**, 127-139 (2021).
7. Kapitein, L.C. et al. The bipolar mitotic kinesin Eg5 moves on both microtubules that it crosslinks. *Nature* **435**, 114-8 (2005).
8. Wijeratne, S. & Subramanian, R. Geometry of antiparallel microtubule bundles regulates relative sliding and stalling by PRC1 and Kif4A. *Elife* **7**, e32595 (2018).
9. Lim, W.M. et al. Regulation of minimal spindle midzone organization by mitotic kinases. *Nat Commun* **15**, 9213 (2024).
10. Yu, C.H. et al. Central-spindle microtubules are strongly coupled to chromosomes during both anaphase A and anaphase B. *Mol Biol Cell* **30**, 2503-2514 (2019).
11. Vukusic, K. et al. Microtubule Sliding within the Bridging Fiber Pushes Kinetochore Fibers Apart to Segregate Chromosomes. *Dev Cell* **43**, 11-23 e6 (2017).
12. Ris, H. The anaphase movement of chromosomes in the spermatocytes of the grasshopper. *Biol Bull* **96**, 90-106 (1949).
13. Nicklas, R.B. Chromosome movement and spindle birefringence in locally heated cells: interaction versus local control. *Chromosoma* **74**, 1-37 (1979).
14. Pamula, M.C. et al. High-resolution imaging reveals how the spindle midzone impacts chromosome movement. *J Cell Biol* **218**, 2529-2544 (2019).
15. Vukusic, K., Ponjavic, I., Buda, R., Risteski, P. & Tolic, I.M. Microtubule-sliding modules based on kinesins EG5 and PRC1-dependent KIF4A drive human spindle elongation. *Dev Cell* **56**, 1253-1267 e10 (2021).
16. Orr, B. et al. An anaphase surveillance mechanism prevents micronuclei formation from frequent chromosome segregation errors. *Cell Rep* **37**, 109783 (2021).
17. Pereira, A.L. et al. Mammalian CLASP1 and CLASP2 cooperate to ensure mitotic fidelity by regulating spindle and kinetochore function. *Mol Biol Cell* **17**, 4526-42 (2006).
18. Brust-Mascher, I., Sommi, P., Cheerambathur, D.K. & Scholey, J.M. Kinesin-5-dependent poleward flux and spindle length control in Drosophila embryo mitosis. *Mol Biol Cell* **20**, 1749-62 (2009).
19. Rogers, G.C. et al. Two mitotic kinesins cooperate to drive sister chromatid separation during anaphase. *Nature* **427**, 364-70 (2004).
20. Ganem, N.J., Upton, K. & Compton, D.A. Efficient mitosis in human cells lacking poleward microtubule flux. *Curr Biol* **15**, 1827-32 (2005).

566 21. Zhang, D., Rogers, G.C., Buster, D.W. & Sharp, D.J. Three microtubule severing enzymes
567 contribute to the "Pacman-flux" machinery that moves chromosomes. *J Cell Biol* **177**,
568 231-42 (2007).
569 22. Rath, U. et al. The Drosophila kinesin-13, KLP59D, impacts Pacman- and Flux-based
570 chromosome movement. *Mol Biol Cell* **20**, 4696-705 (2009).
571 23. Mukherjee, S. et al. Human Fidgetin is a microtubule severing the enzyme and minus-
572 end depolymerase that regulates mitosis. *Cell Cycle* **11**, 2359-66 (2012).
573 24. Guerreiro, A. et al. WDR62 localizes katanin at spindle poles to ensure synchronous
574 chromosome segregation. *J Cell Biol* **220**, e202007171 (2021).
575 25. Anjur-Dietrich, M.I., Kelleher, C.P. & Needleman, D.J. Mechanical Mechanisms of
576 Chromosome Segregation. *Cells* **10**, 465 (2021).
577 26. Zimyanin, V. & Redemann, S. Microtubule length correlates with spindle length in C.
578 elegans meiosis. *Cytoskeleton (Hoboken)* **81**, 356-368 (2024).
579 27. Canman, J.C. et al. Determining the position of the cell division plane. *Nature* **424**, 1074-
580 8 (2003).
581 28. Ballister, E.R., Aonbangkhen, C., Mayo, A.M., Lampson, M.A. & Chenoweth, D.M.
582 Localized light-induced protein dimerization in living cells using a photocaged dimerizer.
583 *Nat Commun* **5**, 5475 (2014).
584 29. Zhang, H. et al. Optogenetic control of kinetochore function. *Nat Chem Biol* **13**, 1096-
585 1101 (2017).
586 30. Chen, G.Y. et al. Tension promotes kinetochore-microtubule release by Aurora B kinase.
587 *J Cell Biol* **220**, e202007030 (2021).
588 31. Chen, G.Y. & Lampson, M.A. Chemical tools for dissecting cell division. *Nat Chem Biol* **17**,
589 632-640 (2021).
590 32. Hunter, A.W. et al. The kinesin-related protein MCAK is a microtubule depolymerase
591 that forms an ATP-hydrolyzing complex at microtubule ends. *Mol Cell* **11**, 445-57 (2003).
592 33. Valdez, V.A., Neahring, L., Petry, S. & Dumont, S. Mechanisms underlying spindle
593 assembly and robustness. *Nat Rev Mol Cell Biol* **24**, 523-542 (2023).
594 34. Oriola, D., Needleman, D.J. & Brugues, J. The Physics of the Metaphase Spindle. *Annu*
595 *Rev Biophys* **47**, 655-673 (2018).
596 35. Khodjakov, A., Copenagle, L., Gordon, M.B., Compton, D.A. & Kapoor, T.M. Minus-end
597 capture of preformed kinetochore fibers contributes to spindle morphogenesis. *J Cell*
598 *Biol* **160**, 671-83 (2003).
599 36. Deng, C. et al. Conditional Localization Pharmacology Manipulates the Cell Cycle with
600 Spatiotemporal Precision. *BioRxiv*, 612697 (2024).
601 37. Neef, R. et al. Choice of Plk1 docking partners during mitosis and cytokinesis is
602 controlled by the activation state of Cdk1. *Nat Cell Biol* **9**, 436-44 (2007).
603 38. Mollinari, C. et al. PRC1 is a microtubule binding and bundling protein essential to
604 maintain the mitotic spindle midzone. *J Cell Biol* **157**, 1175-86 (2002).
605 39. Lansky, Z. et al. Diffusible crosslinkers generate directed forces in microtubule networks.
606 *Cell* **160**, 1159-68 (2015).
607 40. Gaska, I., Armstrong, M.E., Alfieri, A. & Forth, S. The Mitotic Crosslinking Protein PRC1
608 Acts Like a Mechanical Dashpot to Resist Microtubule Sliding. *Dev Cell* **54**, 367-378 e5
609 (2020).

610 41. Braun, M. et al. Adaptive braking by Ase1 prevents overlapping microtubules from
611 sliding completely apart. *Nat Cell Biol* **13**, 1259-64 (2011).
612 42. Janson, M.E. et al. Crosslinkers and motors organize dynamic microtubules to form
613 stable bipolar arrays in fission yeast. *Cell* **128**, 357-68 (2007).
614 43. Desai, A., Maddox, P.S., Mitchison, T.J. & Salmon, E.D. Anaphase A chromosome
615 movement and poleward spindle microtubule flux occur At similar rates in Xenopus
616 extract spindles. *J Cell Biol* **141**, 703-13 (1998).
617 44. Murray, A.W., Desai, A.B. & Salmon, E.D. Real time observation of anaphase in vitro.
618 *Proc Natl Acad Sci U S A* **93**, 12327-32 (1996).
619 45. Laband, K. et al. Chromosome segregation occurs by microtubule pushing in oocytes.
620 *Nat Commun* **8**, 1499 (2017).
621 46. Dumont, J., Oegema, K. & Desai, A. A kinetochore-independent mechanism drives
622 anaphase chromosome separation during acentrosomal meiosis. *Nat Cell Biol* **12**, 894-
623 901 (2010).
624 47. Nahaboo, W., Zouak, M., Askjaer, P. & Delattre, M. Chromatids segregate without
625 centrosomes during Caenorhabditis elegans mitosis in a Ran- and CLASP-dependent
626 manner. *Mol Biol Cell* **26**, 2020-9 (2015).
627 48. Spurck, T.P. et al. UV microbeam irradiations of the mitotic spindle. II. Spindle fiber
628 dynamics and force production. *J Cell Biol* **111**, 1505-18 (1990).
629 49. Spurck, T., Forer, A. & Pickett-Heaps, J. Ultraviolet microbeam irradiations of epithelial
630 and spermatocyte spindles suggest that forces act on the kinetochore fibre and are not
631 generated by its disassembly. *Cell Motil Cytoskeleton* **36**, 136-48 (1997).
632 50. Nicklas, R.B. The motor for poleward chromosome movement in anaphase is in or near
633 the kinetochore. *J Cell Biol* **109**, 2245-55 (1989).
634 51. Redemann, S. et al. C. elegans chromosomes connect to centrosomes by anchoring into
635 the spindle network. *Nat Commun* **8**, 15288 (2017).
636 52. Carlini, L., Renda, F., Pamula, M.C., Khodjakov, A. & Kapoor, T.M. Coupling of
637 microtubule bundles isolates them from local disruptions to set the structural stability of
638 the anaphase spindle. *Proc Natl Acad Sci U S A* **119**, e2204068119 (2022).
639 53. Suresh, P., Long, A.F. & Dumont, S. Microneedle manipulation of the mammalian spindle
640 reveals specialized, short-lived reinforcement near chromosomes. *Elife* **9**, e53807
641 (2020).
642 54. Elting, M.W., Prakash, M., Udy, D.B. & Dumont, S. Mapping Load-Bearing in the
643 Mammalian Spindle Reveals Local Kinetochore Fiber Anchorage that Provides
644 Mechanical Isolation and Redundancy. *Curr Biol* **27**, 2112-2122 e5 (2017).
645 55. Kajtez, J. et al. Overlap microtubules link sister k-fibres and balance the forces on bi-
646 oriented kinetochores. *Nat Commun* **7**, 10298 (2016).
647 56. Sikirzhytski, V. et al. Microtubules assemble near most kinetochores during early
648 prometaphase in human cells. *J Cell Biol* **217**, 2647-2659 (2018).
649 57. Renda, F. et al. Non-centrosomal microtubules at kinetochores promote rapid
650 chromosome biorientation during mitosis in human cells. *Curr Biol* **32**, 1049-1063 e4
651 (2022).
652 58. Lecland, N. & Luders, J. The dynamics of microtubule minus ends in the human mitotic
653 spindle. *Nat Cell Biol* **16**, 770-8 (2014).

654 59. Petry, S., Groen, A.C., Ishihara, K., Mitchison, T.J. & Vale, R.D. Branching microtubule
655 nucleation in Xenopus egg extracts mediated by augmin and TPX2. *Cell* **152**, 768-77
656 (2013).
657 60. Alfaro-Aco, R., Thawani, A. & Petry, S. Biochemical reconstitution of branching
658 microtubule nucleation. *Elife* **9**, e49797 (2020).
659 61. Almeida, A.C. et al. Augmin-dependent microtubule self-organization drives kinetochore
660 fiber maturation in mammals. *Cell Rep* **39**, 110610 (2022).
661 62. Stimac, V., Koprivec, I., Manenica, M., Simunic, J. & Tolic, I.M. Augmin prevents
662 merotelic attachments by promoting proper arrangement of bridging and kinetochore
663 fibers. *Elife* **11**, e83287 (2022).
664 63. Haren, L., Gnadt, N., Wright, M. & Merdes, A. NuMA is required for proper spindle
665 assembly and chromosome alignment in prometaphase. *BMC Res Notes* **2**, 64 (2009).
666 64. Yang, Z., Tulu, U.S., Wadsworth, P. & Rieder, C.L. Kinetochore dynein is required for
667 chromosome motion and congression independent of the spindle checkpoint. *Curr Biol*
668 **17**, 973-80 (2007).
669 65. Yoshida, M.W., Yamada, M. & Goshima, G. Moss Kinesin-14 KCBP Accelerates Chromatid
670 Motility in Anaphase. *Cell Struct Funct* **44**, 95-104 (2019).
671 66. Hu, C.K., Coughlin, M., Field, C.M. & Mitchison, T.J. KIF4 regulates midzone length during
672 cytokinesis. *Curr Biol* **21**, 815-24 (2011).
673 67. Kunchala, P. et al. Plasticity of the mitotic spindle in response to karyotype variation.
674 *Curr Biol* **34**, 3416-3428 e4 (2024).
675 68. Uehara, R. et al. Aurora B and Kif2A control microtubule length for assembly of a
676 functional central spindle during anaphase. *J Cell Biol* **202**, 623-36 (2013).
677 69. Rizk, R.S., Discipio, K.A., Proudfoot, K.G. & Gupta, M.L., Jr. The kinesin-8 Kip3 scales
678 anaphase spindle length by suppression of midzone microtubule polymerization. *J Cell*
679 *Biol* **204**, 965-75 (2014).
680 70. Straight, A.F., Sedat, J.W. & Murray, A.W. Time-lapse microscopy reveals unique roles
681 for kinesins during anaphase in budding yeast. *J Cell Biol* **143**, 687-94 (1998).
682 71. Arquint, C., Gabryjonczyk, A.M. & Nigg, E.A. Centrosomes as signalling centres. *Philos*
683 *Trans R Soc Lond B Biol Sci* **369**, 20130464 (2014).
684 72. Pollard, T.D. Nine unanswered questions about cytokinesis. *J Cell Biol* **216**, 3007-3016
685 (2017).
686 73. Dumont, S. & Mitchison, T.J. Force and length in the mitotic spindle. *Curr Biol* **19**, R749-
687 61 (2009).
688 74. Khandelia, P., Yap, K. & Makeyev, E.V. Streamlined platform for short hairpin RNA
689 interference and transgenesis in cultured mammalian cells. *Proc Natl Acad Sci U S A* **108**,
690 12799-804 (2011).
691 75. Andrews, P.D. et al. Aurora B regulates MCAK at the mitotic centromere. *Dev Cell* **6**, 253-
692 68 (2004).
693 76. Subramanian, R., Ti, S.C., Tan, L., Darst, S.A. & Kapoor, T.M. Marking and measuring
694 single microtubules by PRC1 and kinesin-4. *Cell* **154**, 377-90 (2013).
695 77. Gillingham, A.K. & Munro, S. The PACT domain, a conserved centrosomal targeting motif
696 in the coiled-coil proteins AKAP450 and pericentrin. *EMBO Rep* **1**, 524-9 (2000).
697
698

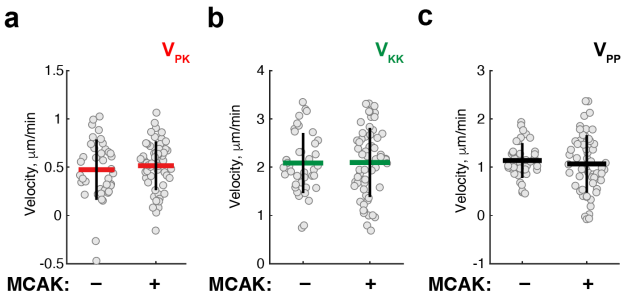

Supplementary Figure 1. MCAK overexpression does not affect motions of chromosomes and poles. Velocities of kMT depolymerization (a), kinetochore separation (b), and pole separation (c) were measured for cells expressing mScarlet-eDHFR (–MCAK, n=40 cells), or MCAK-mScarlet-eDHFR (+MCAK, n=58 cells) as in Fig. 2c-d. For +MCAK cells, data were replotted from –dimerizer cells in Fig. 2e-g. Each data point represents a single cell. Lines: mean ± SD.

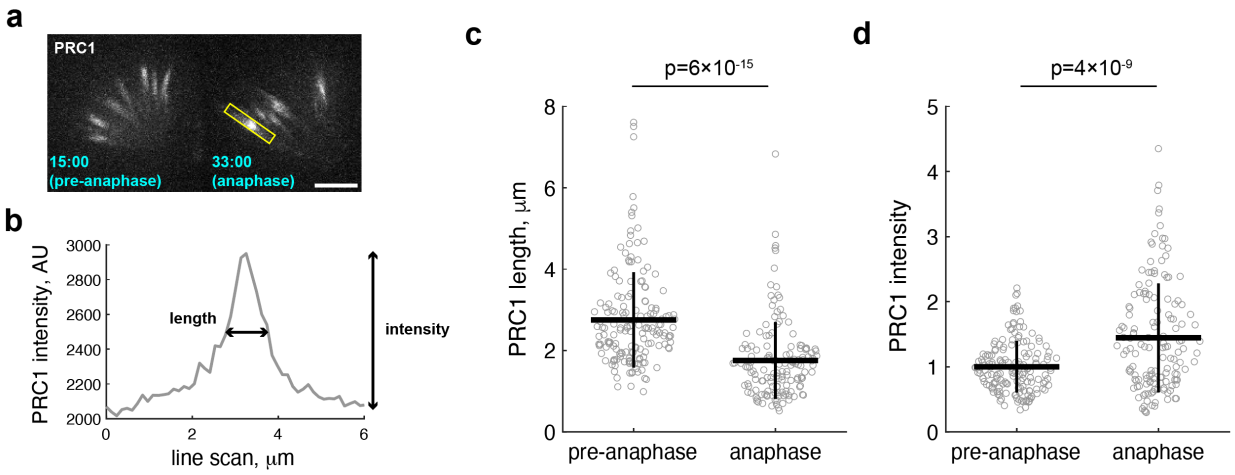

Supplementary Figure 2. PRC1 morphology in monopolar spindles. (a) Representative images of PRC1 bundles before (left) or after (right) anaphase onset. Time stamps indicate the time after uncaging. Scale bars, 5 μm. **(b)** An example of PRC1 intensity analyzed by line scan (box in a). Bundle length and intensity are defined by the full width at half-maximum and the peak height, respectively. **(c-d)** Analyses for bundle length (c) and intensity (d). Each dot represents a PRC1 bundle (n = 162 for pre-anaphase bundles and 148 for anaphase bundles from 23 cells). Lines: mean ± SD.

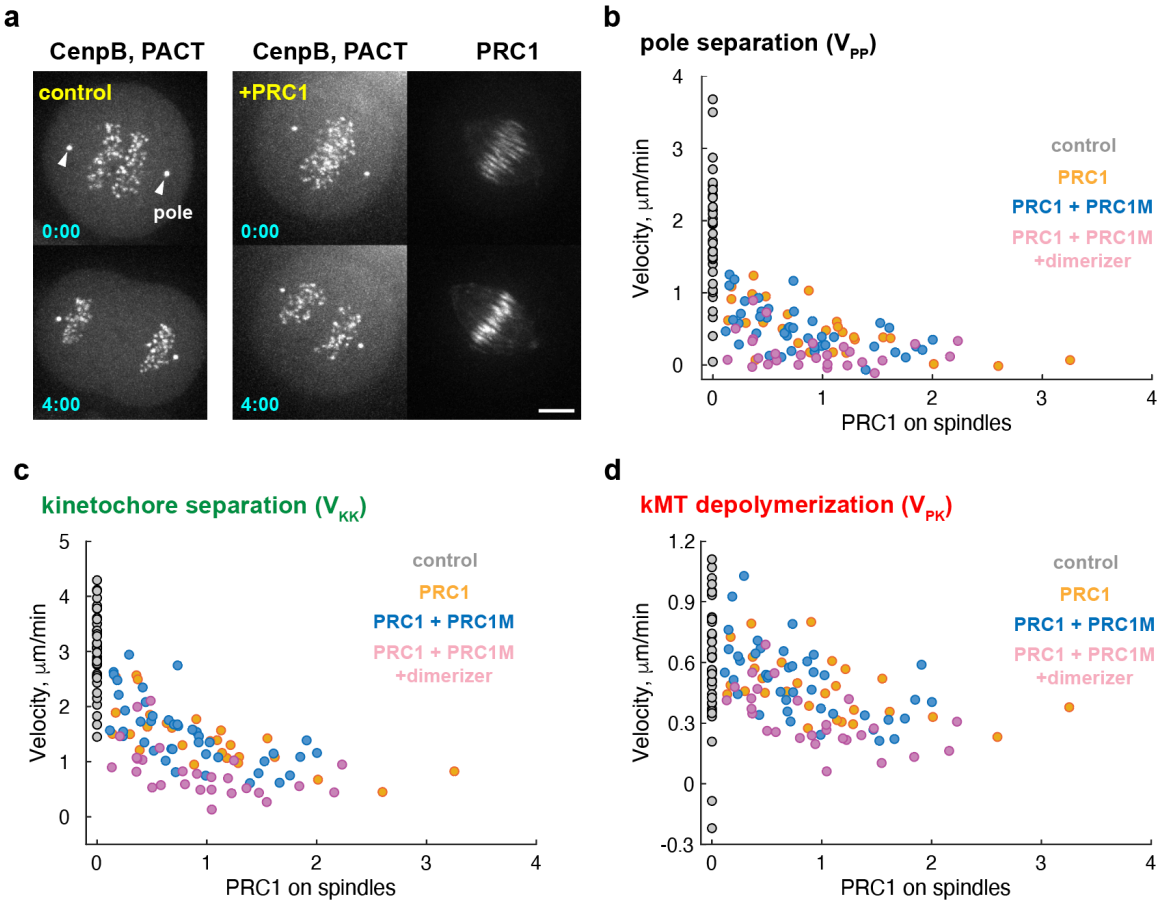

Supplementary Figure 3. PRC1 overexpression and formation of brake complexes inhibit kMT depolymerization. (a) Representative images of cells expressing CenpB-GFP and PACT-GFP, with or without expression of Halo-670nano3-PRC1. Time stamps (min:s) indicate time after first observing sister kinetochore separation at t=0. Scale bars, 5 μm. **(b-d)** Dependence of pole separation (b), kinetochore separation (c), and kMT depolymerization (d) velocities on spindle-bound Halo-670nano3-PRC1. Colored data points show control cells without Halo-670nano3-PRC1 or mScarlet-eDHFR-PRC1M (gray), cells expressing Halo-670nano3-PRC1 (orange), cells expressing Halo-670nano3-PRC1 and mScarlet-eDHFR-PRC1M without dimerization (blue), and cells expressing Halo-670nano3-PRC1 and mScarlet-eDHFR-PRC1M with dimerization (pink). All cells express CenpB-GFP and PACT-GFP. Each data point represents a single cell.

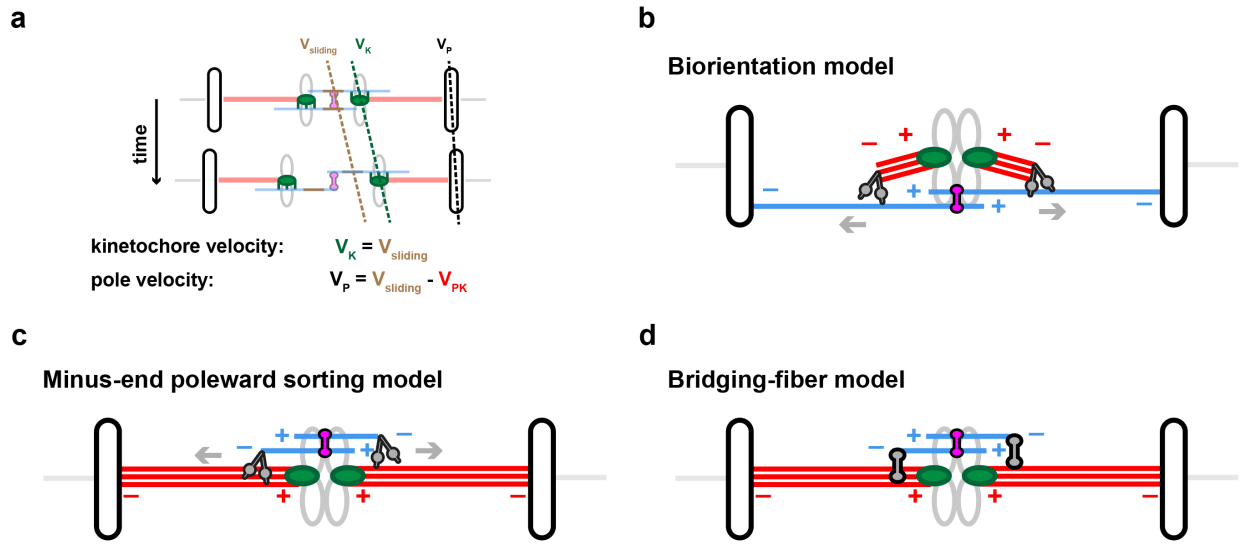

Supplementary Figure 4. Velocity relationships predicted by the sort-and-grip model and proposed mechanisms of parallel sorting. (**a**) Schematic shows kinetochore velocity (V_K), pole velocity (V_P), and antiparallel sliding in the central spindle ($V_{sliding}$). Kinetochore and pole velocities are half of the velocities of kinetochore separation (V_{KK}) and pole separation (V_{PP}), respectively, as measured in Figs. 2 and 4. Kinetochores, poles, and fiducial marks that label antiparallel sliding are shown in green, black, and brown, respectively. In the sort-and-grip model, kinetochore velocity matches sliding velocity, and pole velocity is sliding velocity (moving poles outward) subtracting kMT depolymerization from either end (V_{PK}, moving poles inward). Manipulations of kMT depolymerization affect pole velocity but not kinetochore velocity in this model. (**b**) Kinetochore-nucleated kMT fragments (red) have their plus-ends at kinetochores. Minus-end directed motors (gray) at the minus-ends of these short kMTs preferentially guide kMT growth toward the minus ends of parallel microtubules in the central spindle (blue) to biorient sister kinetochores. (**c**) Minus-end directed motors (gray) guide the minus ends of newly-grown microtubules in the central spindle toward spindle poles through kMTs. (**d**) A fraction of the central spindle is grown by microtubules branching from kMTs (gray). These branching microtubules form antiparallel bundles (bridging fibers) between the two sister kinetochores, bound by antiparallel couplers.

752 **Supplementary Video 1.** Max-intensity projection over 1 μm for the cell shown in Fig.
753 1e. Time stamps (min:s) indicate time after uncaging at t=0. White arrows: spindle pole;
754 scale bar: 10 μm.
755
756 **Supplementary Video 2.** Max-intensity projection over 4 μm for the cells shown in Fig.
757 2b, with (right) or without (left) dimerization. Time stamps (min:s) indicate time after
758 uncaging at t=0. White arrows: spindle pole; scale bar: 5 μm.
759
760 **Supplementary Video 3.** Max-intensity projection over 2 μm showing the off-bundle
761 sister kinetochore pair (yellow arrow) indicated by the gray box in Fig. 3c. Time stamps
762 (min:s) indicate time after uncaging at t=0. Scale bar: 5 μm.
763
764 **Supplementary Video 4.** Max-intensity projection over 2 μm showing the on-bundle
765 sister kinetochore pair (yellow arrow) indicated by the orange box in Fig. 3c. Time
766 stamps (min:s) indicate time after uncaging at t=0. Scale bar: 5 μm.
767
768 **Supplementary Video 5.** Max-intensity projection over the whole cell for the cells
769 shown in Fig. 4c. Left: –dimerizer; Right: +dimerizer. Time stamps (min:s) indicate time
770 after uncaging at t=0. White arrows: spindle pole; scale bar: 5 μm.
771
772 **Supplementary Video 6.** Max-intensity projection over the whole cell for the cells
773 shown in Supplementary Fig. 3a, with (right) or without (left) expression of Halo-
774 670nano3-PRC1. Time stamps (min:s) indicate time after first observing sister
775 kinetochore separation at t=0. White arrows: spindle pole; scale bar: 5 μm.